Microfluidics and Nanofluidics (2025) 29:12
https://doi.org/10.1007/s10404-025-02787-7

RESEARCH

Advancing micromixing techniques: the role of surface acoustic waves and fluid–structure interaction in non-newtonian fluids

Vahid Rabiei Faradonbeh[1] · Soheil Salahshour[2,3,4] · Davood Toghraie[5]

Received: 6 November 2024 / Accepted: 22 January 2025 / Published online: 4 February 2025

Abstract

This study numerically investigated the enhancement of micromixing efficiency through integrating surface acoustic waves (SAWs) and hyper-elastic channel walls, modeled using a power-law fluid representative of human blood flow. The governing equations are systematically divided into zeroth, first, and second orders based on perturbation theory. This facilitates the development of a fully coupled two-way fluid–structure interaction (FSI) framework implemented via the Arbitrary Lagrangian–Eulerian (ALE) method. The combination of SAWs and hyper-elastic materials demonstrated a marked improvement in mixing efficiency, increasing from 0 to 0.99, alongside a significant reduction in pressure drop within the microchannel. The interaction between SAWs and the deformable walls induces localized instabilities and shear stresses that effectively disrupt the laminar flow, promoting enhanced mixing. The study highlights the critical role of hyper-elastic walls in modulating normal forces on the fluid and reducing pressure drop, offering insights into the interaction between fluid viscosity, acoustic pressure fields, and flow dynamics. These findings provide a framework for designing micromixers with optimized efficiency and reduced channel length, offering practical advancements in microfluidic systems.

Keywords Micromixing · Surface acoustic waves (SAWs) · Hyper-elastic materials · Power-law fluid model · Fluid–structure interaction (FSI) · Perturbation theory

List of symbols

c	Concentration (mol/m^3)
d_0	Characteristic displacement (m)
D	Diffusion constant (m^2/s)
f	Excitation frequency (Hz)
p	Pressure (Pa)
$\boldsymbol{v}$	Velocity vector (m/s)
W_H	Mixing channel height (m)
L	Mixing channel length (m)
W	Mixing channel width (m)
n	Power-law index of fluid flow
T	Temperature
I	Identity matrix
WS	The elastic strain energy density (J/m^3)

Greek symbols

$\dot{\gamma}$	Shear rate (s^{-1})
η	Mixing efficiency
μ	Dynamic viscosity (Pas)
ρ	Density (kg/m^3)
λ	Dimensionless Hyper-elastic channel's thickness

Subscript

0	Zeroth-order parameters
1	First-order parameters
2	Second-order parameters
B	Bulk
y	Y-direction
z	Z-direction
Lag	Lagrangian
Eul	Eulerian

✉ Davood Toghraie
Toghraee@iaukhsh.ac.ir

[1] Department of Mechanical Engineering, Science and Research Branch, Islamic Azad University, Tehran, Iran

[2] Faculty of Engineering and Natural Sciences, Istanbul Okan University, Istanbul, Turkey

[3] Faculty of Engineering and Natural Sciences, Bahcesehir University, Istanbul, Turkey

[4] Faculty of Science and Letters, Piri Reis University, Tuzla, Istanbul, Turkey

[5] Department of Mechanical Engineering, Khomeinishahr Branch, Islamic Azad University, Khomeinishahr, Iran

1 Introduction

Micromixers are vital components of microfluidic systems and are typically classified into active and passive categories. Active micromixers leverage external forces—such as electric, magnetic, or acoustic fields—making them particularly suitable for high-precision applications(Ababneh et al. 2023; Bazaz et al. 2024; Wang and Zhang 2024; Oh and Lee 2024; Zheng et al. 2024). In contrast, passive micromixers rely on their geometric design to induce chaotic advection or promote laminar flow, achieving efficient mixing without external energy sources (Yin 2023). Recent advancements have introduced hybrid systems that combine the precision of active methods with the simplicity and energy efficiency of passive designs, offering a versatile solution for various microfluidic applications (Kharaji and Bayareh 2024; Li et al. 2024; Ferreira et al. 2024; Meng and Wu 2023). While active micromixers can be powerful, they often involve complex fabrication techniques and substantial energy inputs (Afzal 2021). Conversely, passive micromixers are more cost-effective and more accessible to implement (Chen et al. 2018). Research has shown that hybrid designs, especially those integrating acoustic fields, can significantly enhance mixing efficiency in both biological and chemical contexts, improving performance in complex processes (Bayareh et al. 2020). Innovative designs, such as dielectric stack actuators, have emerged to provide both mixing and pumping capabilities, enhancing their applicability in lab-on-a-chip systems and potentially revolutionizing the field (Solano-Arana et al. 2018). These developments are critical for optimizing fluid dynamics and improving the functionality of microfluidic devices (Bai et al. 2024). Incorporating hyper-elastic materials into microfluidic designs offers substantial advantages, particularly in accurately modeling biological tissues and enhancing device functionality. Hyper-elastic materials, such as poly(N-isopropyl acrylamide) (PNIPAm) microgels, exhibit significant deformation capabilities that mimic biological tissues under various stress conditions (Hussain et al. 2023). Hyperbolic microchannels allow for improved measurement of cell viscoelasticity, providing a straightforward stress–strain relationship that enhances mechanical evaluations(Reichel et al. 2024). Furthermore, hyper-elastic materials play a crucial role in the development of multi-axial strain and contact pressure sensors, which are essential for applications in soft robotics and environmental interactions(Kumar and Pandey 2022). Recent advancements have included microfluidic devices with hyper-elastic valves that automate glucose stimulation and insulin collection from pancreatic islets, showcasing the versatility of hyper-elastic materials in biological applications(Quintard et al. 2022). However, scaling these technologies for widespread industrial use presents challenges, particularly regarding user-friendliness and reliability in complex biological environments. Integrating surface acoustic waves (SAWs) into microfluidic systems significantly enhances micromixing efficiency, offering numerous benefits for biomedical applications. SAW technology exploits acoustic streaming and particle manipulation, improving mixing and reaction rates(Ghorbani Kharaji et al. 2021). By facilitating active mixing through acoustic streaming, SAWs promote rapid and uniform distribution of reactants within microfluidic channels (Bai et al. 2022). The use of standing surface acoustic waves allows for precise control over particle manipulation, enabling effective sorting and trapping of microparticles, which is crucial for diagnostic applications (Mezzanzanica et al. 2022). Additionally, SAW technology enables non-contact manipulation of bioparticles, enhancing biocompatibility and scalability in lab-on-a-chip systems (Qi et al. 2024). The incorporation of acoustically reflective surfaces can increase energy retention, resulting in higher flow rates and improved capture efficiencies for nanoparticles (Ang et al. 2023). Despite the advantages of SAW-based micromixing, challenges such as thermal effects and the need for optimized channel designs remain critical for maximizing performance in practical applications. By leveraging acoustic streaming and secondary flow patterns, SAW micromixing techniques significantly enhance the mixing behavior of non-Newtonian fluids in microchannels. These methods improve mixing efficiency, particularly for pseudoplastic fluids, which typically exhibit lower mixing performance than dilatant fluids. Acoustic streaming induced by SAWs generates localized microstreaming that disrupts fluid interfaces and promotes chaotic advection, leading to improved mixing (Saravanakumar and Cicek 2023). Secondary flows in devices like the Two-Layer Crossing Channels Micromixer (TLCCM) enhance mixing performance, achieving mixing degrees between 0.80526 and 0.99765 for pseudoplastic fluids (Kouadri et al. 2024). The viscosity and flow behavior index (n) of the fluid influence mixing efficiency, Pseudoplastic fluids ($n < 1$), while exhibiting shear-thinning behavior and lower resistance to flow under shear, generally mix less effectively than dilatant fluids ($n > 1$). Pseudoplastic fluids, characterized by their shear-thinning behavior, typically exhibit lower viscosity and reduced flow resistance under shear compared to dilatant fluids. However, this lower viscosity can pose challenges in specific micromixing applications, as it limits the formation and stability of robust secondary flow structures, such as vortices. These structures are crucial for enhancing mixing efficiency by promoting fluid layer interactions and chaotic advection. Consequently, the reduced viscous dissipation in pseudoplastic fluids may result in weaker flow

dynamics, hindering the development of effective mixing patterns. This highlights the importance of considering the rheological properties of pseudoplastic fluids when designing micromixers to optimize mixing performance (Bansal et al. 2023). Although SAW techniques promise to improve micromixing, challenges in balancing power consumption and fluid compatibility necessitate further research to optimize these systems for various non-Newtonian fluids. The effect of hyper-elastic channel walls on micromixing is substantial, as these walls can enhance mixing efficiency through several mechanisms. Integrating elastic materials within microchannels allows for dynamic flow manipulation, essential for effective micromixing Electrokinetic instabilities generated by elastic walls can lead to local electro-elastic turbulence when subjected to an electric field, resulting in chaotic flow patterns that improve the mixing of viscoelastic fluids (Sasmal 2022).

Additionally, the deformation of elastic walls in response to vibrational pressure creates swirling flows, further enhancing the interaction between fluid layers (Takayama et al. 2021). However, challenges like wall slip in viscoelastic fluids can impede particle ordering and mixing efficiency (D'Avino and Maffettone 2022). Therefore, careful design is crucial to optimize the benefits of hyper-elastic materials in microfluidic applications. In conclusion, using surface acoustic waves (SAWs) significantly enhances the mixing of non-Newtonian fluids in microfluidic devices through various physical mechanisms. This enhancement is primarily attributed to acoustic streaming and the generation of vortices, which facilitate improved fluid interaction. SAWs induce acoustic streaming that creates flow patterns, enhancing mixing efficiency. This phenomenon is especially effective in vertical-type SAW mixers, where the induced vortices act as hydrodynamic barriers, promoting controlled mixing of co-flowing streams. Cha et al. (2023) presented a novel approach to microfluidic mixing using ultrasonic surface acoustic wave (SAW)-induced acoustic streaming flow (ASF). Unlike traditional cross-type SAW mixers, which primarily utilize horizontal acoustic forces, this study introduces a vertical-type SAW mixer that enhances mixing efficiency and controllability by leveraging the vertical component of the acoustic force. The authors conducted extensive numerical simulations and experimental investigations to explore acoustic-hydrodynamic phenomena under various conditions, including total flow rate, acoustic wave amplitude, and fluid viscosity. Their findings indicate that SAW-induced vortices act as hydrodynamic barriers, facilitating controlled mixing of co-flowing streams. The research also demonstrates a proof-of-concept application involving rapid red blood cell lysis, achieving high lysis efficiency through physical interactions of suspended cells with acoustic vortical flows. This vertical-type ultrasonic SAW mixer shows promise for a wide range of microfluidic applications requiring rapid and controlled mixing, highlighting its potential impact in microfluidics. Efficient chaotic microdevices are crucial in various industrial applications, particularly in microfluidics. The Two-Layer Crossing Channels Micromixer (TLCCM) has demonstrated significant advantages in mixing Newtonian fluids, prompting a comparative analysis with other micromixers when employing pseudoplastic fluids. Kouadri et al. (2024) utilized computational fluid dynamics (CFD) to solve the Navier–Stokes equations, mass conservation, and species transport equations, focusing on the mixing process of carboxymethyl cellulose (CMC) solutions characterized by a power-law model. Their research revealed that the TLCCM micromixer achieved a remarkable mixing degree ranging from 0.80526 to 0.99765, outperforming other micromixers such as L-Shape, OH, and OX. Additionally, the presence of secondary flows was found to enhance mixing performance while requiring lower energy costs, which varied between 0.00036 and 0.49 W. These findings underscore the TLCCM's potential for improved mixing efficiency in microfluidic applications, emphasizing its effectiveness in handling non-Newtonian pseudoplastic fluids. Introducing heterogeneous wall properties, such as varying zeta potential, can enhance mixing by generating rotational currents. This approach improves mixing efficiency compared to homogeneous walls, particularly at higher Reynolds numbers. Farahinia et al. (2021) explored the impact of heterogeneous surface properties on mixing efficiency in microfluidic systems. Their research highlights that traditional mixing in microchannels with homogeneous walls relies heavily on molecular diffusion, often insufficient for achieving thorough mixing. The authors propose utilizing electroosmotic flow characteristics combined with strategically designed heterogeneous zeta-potential patches on microchannel walls to address this limitation. Their findings indicate that the length and positioning of these patches significantly influence mixing performance, with the slip coefficient on the wall playing a more critical role than variations in Reynolds number. The study reveals that while a homogeneous channel may be preferable at low Reynolds numbers, introducing heterogeneity at increased Reynolds numbers can enhance mixing efficiency. However, caution is advised, as a higher slip coefficient can lead to a sharp decline in mixing efficiency in high Reynolds number scenarios. This research provides valuable insights into optimizing microfluidic mixing processes, emphasizing the importance of surface chemistry in enhancing electroosmotic flow dynamics. A combination of advanced modeling techniques and computational platforms is essential for numerically solving Acoustofluidic and fluid–structure interaction (FSI) problems. Recent research highlights effective strategies based on these methods. Implementing an acoustic FSI formulation in the open-source MOOSE platform has been verified and validated against analytical solutions and

experimental data. This demonstrates its capability for seismic analysis of fluid-filled structures. The acoustic fluid–structure interaction (FSI) formulation serves as a practical numerical approach for the seismic analysis of fluid-filled tanks. However, no verification and validation studies reported in the literature have demonstrated the ability of an acoustic FSI numerical model to predict responses critical to structural and mechanical design under intense translational and rotational earthquake inputs. Dhulipala et al. (2022) presented an acoustic FSI formulation implemented in the open-source Multiphysics Object-Oriented Simulation Environment (MOOSE), formally verified and validated using analytical solutions for small amplitude, unidirectional seismic inputs. The code-to-code verification utilizes a previously verified and validated Arbitrary Lagrangian–Eulerian (ALE) numerical model in the commercial finite element code LS-DYNA. Validation studies utilize a comprehensive dataset assembled from the results of 3D earthquake-simulator tests of a fluid-filled vessel. The acoustic numerical model in MOOSE is verified and validated for hydrodynamic pressures and support reactions, except in cases involving significant convective responses. For small amplitude inputs, numerically predicted wave heights match those of the analytical solutions. However, the model is not verified and validated for wave height calculations under intense 3D seismic inputs. The run times for the acoustic FSI simulations in MOOSE are an order of magnitude shorter than the corresponding ALE simulations in LS-DYNA. The utility of the MOOSE acoustic FSI implementation is demonstrated by conducting a seismic analysis of a building equipped with a fluid-filled, advanced nuclear reactor. In summary, Lei et al. (2020) presented a comprehensive study on the innovative use of acoustic microfluidic systems for the continuous separation of microparticles. Their work employs numerical simulations to explore the dynamics of microparticle behavior in a two-stage system, enhancing the efficiency of separation processes. Usefian and Bayareh (2020) focused on evaluating the mixing quality of a novel micromixer made from PDMS, with the primary objective of proposing an efficient design for low-Reynolds-number flows. The study investigated how various factors, including inlet velocity (Reynolds number), the number of mixing cycles, and blockage ratio, influenced the micromixer's performance, aiming to enhance its applicability in practical microfluidic systems. To achieve these objectives, the authors employed a combination of experimental and numerical methods, fabricating the micromixer and conducting experiments to assess its mixing efficiency while validating the results through numerical simulations. This comprehensive approach allowed for a detailed analysis of the micromixer's behavior under different operational conditions, particularly focusing on flow dynamics and mixing performance. The results indicated that mixing efficiency (ME) improved with increased injection velocities, more mixing cycles, and higher blockage ratios, with the micromixer achieving a remarkable 100% mixing efficiency at a blockage ratio of 0.25. Additionally, the study provided specific values for the ratio of mixing efficiency to pressure drop (ME/ΔP), demonstrating that the micromixer with three, four, five, and six mixing cycles had ME/ΔP values of 6.36, 2.23, 0.74, and 0.5, respectively. These findings highlighted the micromixer's potential for practical applications, particularly in scenarios where the Reynolds number was less than 75. Usefian et al. (2019) investigated the mixing quality of an electro-osmotic micro-mixer. They designed a microchamber featuring an electrode array symmetrically placed on its surface, along with an inner cylindrical obstacle. The methodology involved performing simulations to determine the optimal radius for the inner cylinder, while also examining various parameters such as AC frequency, voltage value, liquid inlet velocity, and the angular velocity of the inner cylinder. The results indicated that the application of an electric field significantly enhanced the mixing rate. Specifically, the study found that mixing efficiency increased with higher frequencies, greater voltage values, and increased angular velocities, while it decreased with higher inlet velocities of the fluids. Notably, the mixing efficiency reached 71.02% at an angular velocity of 0.0148 rad/s and improved to 97.67% at 1.148 rad/s. Furthermore, the findings revealed that shear-thinning fluids exhibited better mixingperformance compared to shear-thickening fluids, highlighting the importance of fluid properties in electro-osmotic mixing applications. Peng et al. (2024) investigated the complex rheological properties of viscoelastic fluids in nanochannels, aiming to understand the instabilities that arose during their flow at high Weissenberg numbers. They employed the simplified Phan-Thien-Tanner viscoelastic fluid model and utilized the log-conformation tensor approach to analyze the flow characteristics. By varying key rheological parameters, they observed significant effects on flow behavior and instability. The results revealed that the flow velocity and outlet current exhibited regular periodic fluctuations within a specific range of parameters. As the flow transitioned from a single-vortex state to a symmetric double-vortex state, the average velocity increased by about 15%. Additionally, the researchers noted that increasing the Weissenberg number led to substantial increases in the vortex dimensions, highlighting the importance of rheological properties in the flow dynamics of viscoelastic fluids in nanochannels. Bahrami and Bayareh (2022) proposed a novel micromixer design that combined twisted channel walls with a plane spiral microchannel to enhance mixing efficiency in microfluidic systems. They aimed to overcome the challenges associated with mass transfer in laminar flow conditions, which often impede effective mixing. The methodology involved performing simulations using the finite difference method and

ANSYS FLUENT 2021 software to evaluate the micromixer's performance across various Reynolds numbers. The results revealed that the proposed micromixer achieved a mixing efficiency that was 53% greater than that of a T-shaped twisted microchannel and 51% higher than that of a conventional plane spiral channel for the same Reynolds number. Furthermore, the study indicated that a 3/4 loop of the twisted-spiral microchannel provided a 7.51% improvement in mixing efficiency compared to a one-and-a-half loop of a plane spiral channel. Overall, the innovative design led to a 35% enhancement in mixing quality while maintaining a pressure drop increase of less than 0.5%. These findings highlighted the potential of the novel micromixer to significantly improve mixing performance in various microfluidic applications, marking a valuable advancement in the field of microfluidics. Ghorbani Kharaji et al. (2022) and Mahapatra and Bandopadhyay (2022) focused on investigating the mixing characteristics of an Oldroyd-B fluid flowing through a micro-channel equipped with discrete electrodes, driven by both electroosmotic forces and pressure gradients. The researchers aimed to understand how different potential distributions along the channel walls influenced mixing efficiency. To achieve this, they employed a numerical approach that considered both symmetric and asymmetric potential distributions, while also examining the effects of fluid rheology and various physicochemical parameters on the mixing process. The study revealed that increasing the relative strength of electroosmotic forcing relative to the pressure gradient improved mixing efficiency. Additionally, it was found that localized mixing efficiency decreased with an increase in surface potential, and the five-electrode arrangement yielded mixing efficiencies comparable to continuous distributions. The researchers also noted that increasing the gap between electrodes enhanced mixing efficiency at the micro-channel outlet. Overall, the findings provided valuable insights for the design and analysis of active micromixers, particularly for the efficient transport of bio/polymeric fluids within microchannels highlighting the complex interplay between electroosmotic and pressure-driven flows in optimizing mixing processes. John et al. (2024) investigated the influence of viscoelasticity on mixing efficiency in helical static mixers, which are essential in processing complex formulated products. The researchers employed computational fluid dynamics (CFD) to analyze the flow of a FENE-CR model fluid, focusing on how flow distribution asymmetries developed at the intersections of mixer elements affected mixing performance. They found that increased viscoelasticity hindered mixing efficiency, particularly in the laminar flow regime. The study quantified the degree of flow asymmetry across various conditions, revealing that the asymmetry parameter did not follow the typical pitchfork bifurcation observed in symmetrical geometries. Instead, for low values of the extensibility parameter (L2), the flow remained steady across all Reynolds (Re) and Weissenberg (Wi) numbers studied. However, as L2 increased, the flow transitioned to a transient state, significantly increasing the magnitude of the asymmetry. The researchers utilized a Lagrangian particle tracking technique to quantify mixing performance, introducing a new mixing index based on the mean nearest distance between tracked particle sets. Overall, the findings provided critical insights into the complex relationship between viscoelasticity and mixing processes, enhancing the understanding of their implications in industrial applications. Mahapatra and Bandopadhyay (2023) investigated the impact of geometrically modified microchannels on the micromixing of polymeric solutions. They employed a combination of experimental and numerical analyses to validate the flow characteristics of Newtonian fluids within these modified channels. The methodology included the fabrication of microchannels using stereolithography and the development of an in-house image processing code in MATLAB to analyze dye concentration distributions. The study's results highlighted the occurrence of inertio-elastic instability in the modified microchannels, which significantly enhanced mixing efficiency. This enhancement was attributed to the interaction between the viscoelastic properties of the fluids and the unique geometrical features of the channels. The findings provided important insights into the design and operation of microfluidic devices, particularly for applications involving the transport of bio/polymeric fluids, thereby contributing to the optimization of passive micromixers in microchannels. Babaie et al. (2022) investigated the performance of a novel combination of sinusoidal and serpentine microchannels with two types of sinusoidal walls, aiming to enhance micromixing efficiency. The research employed both numerical and experimental approaches for Reynolds numbers ranging from 0.01 to 100. Three-dimensional steady-state Navier–Stokes equations, coupled with the convection–diffusion equations were solved on a structured mesh to determine the flow field and species concentration distribution. Soft lithography was utilized to fabricate the microchannels using PDMS. The results revealed that the addition of convergent-divergent regions significantly improved the mixing index, achieving a maximum value of 99.89% at $Re = 100$. Furthermore, serpentine-sinusoidal mixers were shown to achieve maximum mixing efficiency with fewer mixing units compared to standard serpentine mixers. The study demonstrated that the enhanced mixing efficiency was primarily due to centrifugal forces, the formation of Dean vortices, and sudden contraction–expansion effects. Additionally, micromixers with a smaller amplitude and a larger number of bumps exhibited higher performance coefficients.

This research is significant as it addresses challenges faced by traditional micromixing methods, offering a practical alternative for various biomedical and industrial

applications. The findings indicate that the acoustic-microfluidic approach can substantially improve microparticle separation efficiency and throughput, highlighting its potential for future research and practical applications in microfluidics. In the realm of microfluidic systems, integrating acoustic wave dynamics with the mechanical characteristics of flexible channel walls represents a critical yet underexplored area of research. Existing literature predominantly addresses Newtonian fluids' acoustic response or rigid channels' structural behavior, often overlooking the complex interplay arising from non-Newtonian fluid dynamics within Hyperelastic materials. Moreover, while the enhancement of mixing efficiency is a well-recognized objective, there is a conspicuous lack of studies that concurrently tackle the challenge of minimizing pressure drop. This vital metric significantly affects the operational efficacy of microfluidic devices. This research aims to bridge this significant gap by employing planar acoustic wave theory and a comprehensive parametric fluid flow model that incorporates Newtonian and non-Newtonian power-law behaviors applied within a Hyperelastic channel framework. By implementing a fully coupled two-way fluid–structure interaction (FSI) solution, this study advances the understanding of how acoustic perturbations can optimize mixing efficiency while effectively addressing pressure loss issues. Such a multifaceted approach enhances the theoretical foundations of microfluidic mixing mechanisms and paves the way for designing next-generation devices that balance performance with energy efficiency. This investigation is poised to contribute valuable insights into the synergistic effects of acoustic waves and structural flexibility, thereby positioning it as a novel and essential contribution to the field of microfluidics.

2 Problem definition and geometry

Figures 1 and 2 illustrate that the micromixer is based on an H-shaped microchannel. To evaluate the effect of the hyperelastic channel wall on the micromixing performance, a fully coupled Fluid–Structure Interaction (FSI) model has been applied to the channel structure. The fluid inside the channel is excited using two surface acoustic wave (SAW) generators

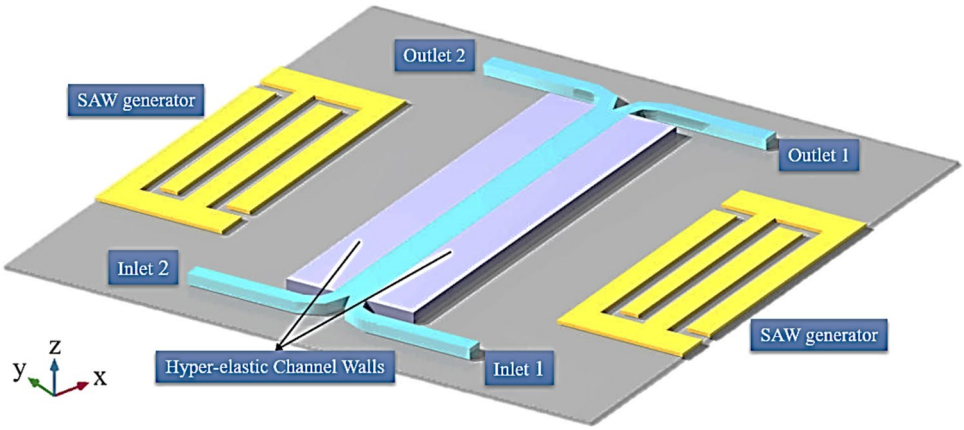

Fig. 1 Schematic of micromixer unit

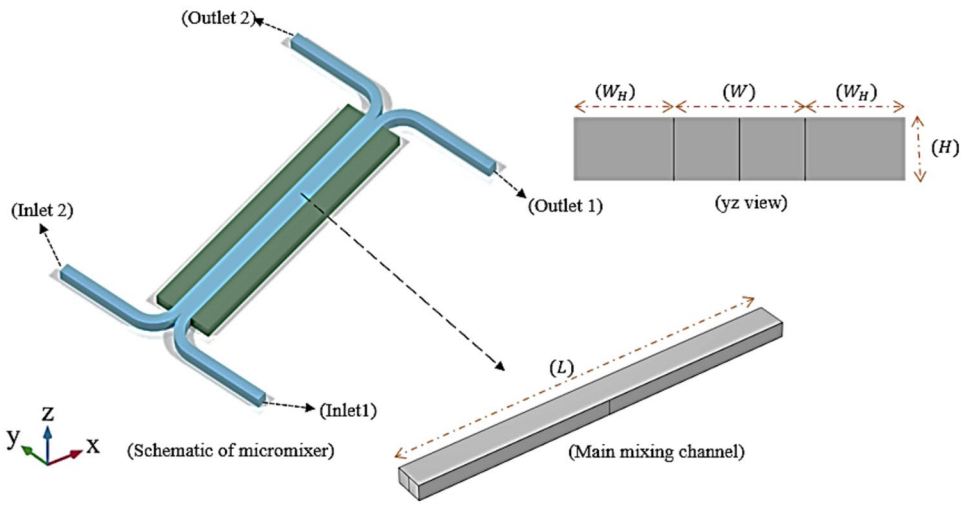

Fig. 2 Micromixer channel's structure

placed on the lateral walls of the channel. The following figure provides a schematic representation of the micromixer configuration utilized in this study.

The micromixer illustrated in Figs. 1 and 2 integrates surface acoustic wave (SAW) technology with a microchannel featuring hyper-elastic walls, providing a novel approach to enhance micromixing efficiency. This design is particularly relevant for applications such as biochemical assays, drug delivery systems, and lab-on-a-chip devices, where efficient mixing is crucial. In Fig. 1, the micromixer is shown with two fluid inlets (Inlet 1 and Inlet 2) and two outlets (Outlet 1 and Outlet 2), where separate fluid streams enter and exit the microchannel. The key feature of this design is the use of hyper-elastic channel walls, which enable fluid–structure interaction (FSI). These walls, made from a flexible material, dynamically deform in response to fluid pressure and acoustic waves. This deformation facilitates more effective fluid mixing by altering the flow patterns inside the channel, especially at low Reynolds numbers where passive mixing methods are typically less efficient. The SAW generators on either side of the channel produce high-frequency surface acoustic waves propagating through the fluid, creating oscillations and chaotic advection. These oscillations disrupt the laminar flow and induce vortices that significantly improve mixing efficiency. Additionally, the interaction between the acoustic waves and the hyper-elastic walls further enhances the mixing process by amplifying the internal fluid motion. Figure 2 provides a more detailed view of the micromixer's geometry, focusing on the dimensions of the main mixing channel, including the channel width (W), wall thickness (W_H), and height (H). The longitudinal structure is depicted, showing the length (L) of the channel where the mixing primarily takes place. The yz cross-sectional view highlights how the hyper-elastic material encapsulates the fluid flow, allowing for adaptive pressure distribution and efficient mixing across the channel's length. The two inlets facilitate the introduction of different fluid streams, which then undergo rapid mixing as they pass through the main channel. Here, the combined effects of SAW-induced oscillations and hyper-elastic wall deformations ensure that the fluids mix thoroughly before exiting through the outlets. The elasticity of the channel walls plays a pivotal role by dynamically responding to fluid pressure and acoustic forces, maintaining a low-pressure drop while optimizing the flow patterns for enhanced mixing. This innovative design overcomes the limitations of traditional passive micromixers by incorporating active mixing mechanisms. The surface acoustic waves actively induce mixing by generating intense oscillations, while the hyper-elastic walls provide a dynamic, responsive structure that further promotes fluid mixing through real-time deformation. This dual mechanism not only improves mixing efficiency but also minimizes pressure losses, a critical aspect in microfluidic systems where maintaining low pressure is essential for system performance. The fully coupled two-way fluid–structure interaction (FSI) between the hyper-elastic walls and the fluid inside the channel ensures efficient energy transfer, enhancing both the mixing performance and the overall flow dynamics. Additionally, the design is scalable and adaptable to various microfluidic applications, including those that require rapid and thorough mixing, such as chemical reactions and biological diagnostics. In conclusion, the micromixer presented in Figs. 1 and 2 demonstrates a cutting-edge approach to microfluidic mixing by combining SAW technology with hyper-elastic materials. The interaction between the acoustic waves and deformable channel walls creates an ideal environment for effective fluid mixing while maintaining low-pressure drop and enabling a compact design. This micromixer provides a highly efficient and innovative solution for a range of applications, offering significant advantages over conventional passive micromixers.

2.1 Governing equations

The problem of background fluid flow, similar to classical computational fluid dynamics (CFD) scenarios, is rigorously defined by the governing conservation equations of mass and momentum, as outlined below (Ramesh et al. 2024). These fundamental equations form the core framework of fluid dynamics, capturing the behavior of fluid in motion. The continuity equation governs mass conservation, while the Navier–Stokes equations handle momentum conservation, accounting for external forces, pressure gradients, and viscous effects. Moreover, by employing perturbation theory due to the introduction of SAWs (Stevenson 2409), the CFD problem is further divided into zeroth-order, first-order, and second-order components. Each set of parameters is represented by a corresponding index, facilitating a structured analysis of the flow field's response to acoustic perturbations. This approach comprehensively explains the fluid's dynamic interactions with acoustic waves under various boundaries and initial conditions (Faradonbeh et al. 2022).

$$\frac{\partial \rho_0}{\partial t} + \rho_0(\nabla.\boldsymbol{v}_0) = 0, \tag{1}$$

$$\rho_0 \frac{\partial \boldsymbol{v}_0}{\partial t} + \rho_0(\boldsymbol{v}_0.\nabla)\boldsymbol{v}_0 = -\nabla p_0 + \mu\nabla^2\boldsymbol{v}_0 + \left(\mu_b + \frac{1}{3}\mu\right)\nabla(\nabla.\boldsymbol{v}_0). \tag{2}$$

In the above equations, the parameters ρ, v, p, and μ represent the fluid's density, velocity field, pressure, and viscosity. To solve the coupled system of Eqs. (1) and (2), parametric velocities (as detailed in Table 1) were applied at the inlet of the micromixer. These velocities are critical for accurately simulating the flow dynamics within the microfluidic environment. Furthermore, at the

Table 1 Parameters Value

Parameter	Value	Description
Channel configuration		
$\boldsymbol{W}$	380 [μm]	Channel width
$\boldsymbol{H}$	160 [μm]	Channel height
$\boldsymbol{L}$	5 [mm]	Channel length
λ	[0,0.5,4]	Hyperelastic channel dimensionless thickness
Power-law model of fluid flow		
$\boldsymbol{m}$	0.0035 [Pa. s]	Fluid flow consistency
$\boldsymbol{n}$	[0.6,0.1,1.4]	Power-law index
$\boldsymbol{D}$	1e-9 [m^2/s]	Diffusion coefficient
$\boldsymbol{cs}$	1578.2 [m/s]	Speed of sound at blood
$\boldsymbol{\mu_B}$	6.4 [Pa. s]	Bulk viscosity
Operational parameters		
$\boldsymbol{vel}$	[0.002,0.001,0.01] [m/s]	Inlet velocity
$\boldsymbol{d}_0$	0.1 [nm]	Acoustic actuation parameters
$\boldsymbol{f}_0$	1.94 [MHz]	Excitation frequency

interface between the solid wall and the fluid, the continuity of stress and velocity was enforced to ensure seamless interaction between the fluid and the hyper-elastic material of the channel walls. This approach is essential for capturing the nuances of Fluid–Structure Interaction (FSI), where the deformability of the wall significantly influences the flow characteristics and, consequently, the mixing efficiency within the micromixer. By maintaining this continuity at the fluid–solid interface, the model accurately reflects the real physical interactions, enhancing the reliability of the simulation results and providing a comprehensive understanding of the micromixing process. The present study uses the power-law fluid flow model (Rubio Martínez et al. 2024) to model the fluid's viscosity, as shown in Eq. (3). The zero index indicates the zeroth order of the background fluid flow and *b* denotes the bulk, considered for the bulk viscosity.

$$\mu = m(\dot{\gamma})^{n-1}. \tag{3}$$

The fluid response to SAWs in the frequency domain is simulated using the thermo-viscous equations. Equations (4), (5), and (6) represent the thermoviscous equations in the frequency domain, derived through the application of perturbation theory to the energy, mass conservation, and momentum conservation equations. Furthermore, applying perturbation theory to the classical mass and momentum conservation equations while retaining the second-order parameters results in the acoustic flow equations presented in (7) and (8). This approach provides a detailed framework for understanding the interplay between acoustic waves and the fluid's thermoviscous behavior (Nalimela et al. 2025), allowing for accurate modeling of their interactions.

$$\frac{\partial T_1}{\partial t} = D_{th}\nabla^2 T_1 + \frac{\alpha T_0}{\rho_0 C_p}\frac{\partial p_1}{\partial t} \tag{4}$$

$$\frac{\partial \rho_1}{\partial t} + \nabla.(\rho_0 \boldsymbol{v}_1 + \rho_1 \boldsymbol{v}_0) = 0 \tag{5}$$

$$\begin{aligned} &\rho_0\frac{\partial \boldsymbol{v}_1}{\partial t} + \rho_1\frac{\partial \boldsymbol{v}_0}{\partial t} + \rho_0(\boldsymbol{v}_1.\nabla)\boldsymbol{v}_0 \\ &+ \rho_0(\boldsymbol{v}_0.\nabla)\boldsymbol{v}_1 + \rho_1(\boldsymbol{v}_0.\nabla)\boldsymbol{v}_0 \\ &= -\nabla p_1 + \mu\nabla^2\boldsymbol{v}_1 + \left(\mu_b + \frac{1}{3}\mu\right)\nabla(\nabla.\boldsymbol{v}_1). \end{aligned} \tag{6}$$

$$< \frac{\partial \rho_2}{\partial t} > + \nabla.(< \rho_0 \boldsymbol{v}_2 > + < \rho_2 \boldsymbol{v}_0 >) = -\nabla.< \rho_1 \boldsymbol{v}_1 > \tag{7}$$

$$\begin{aligned} &< \rho_0\frac{\partial \boldsymbol{v}_2}{\partial t} > + < \rho_2\frac{\partial \boldsymbol{v}_0}{\partial t} > + < \rho_1\frac{\partial \boldsymbol{v}_1}{\partial t} > + < \rho_0\boldsymbol{v}_1.\nabla\boldsymbol{v}_1 > \\ &+ < \rho_0(\boldsymbol{v}_0.\nabla)\boldsymbol{v}_2 > + < \rho_0(\boldsymbol{v}_2.\nabla)\boldsymbol{v}_0 > + < \rho_1(\boldsymbol{v}_0.\nabla)\boldsymbol{v}_1 > \\ &+ < \rho_1(\boldsymbol{v}_1.\nabla)\boldsymbol{v}_0 > + < \rho_2(\boldsymbol{v}_0.\nabla)\boldsymbol{v}_0 > = -\nabla < p_2 > + \mu\nabla^2 < \boldsymbol{v}_2 > \\ &+ \left(\mu_b + \frac{1}{3}\mu\right)\nabla(\nabla.< \boldsymbol{v}_2 >). \end{aligned} \tag{8}$$

The coupling of the system of Eqs. (1) to (8) yields the Acoustofluidic viscous-parametric microfluid flow equations within the micro-mixer unit. The system of Eqs. (4) through (6) was solved by applying the boundary condition of lateral wall excitation (see Figs. 1 and 2) as well as an isothermal boundary condition on all channel walls. The lateral excitation, induced through surface acoustic waves (SAWs), interacts with the fluid flow, creating disturbances that enhance mixing efficiency. The isothermal boundary

condition ensures a uniform temperature distribution along the walls, which is critical for maintaining the consistency of thermal effects during the mixing process. These boundary conditions are integral to accurately modeling the micromixing phenomenon and understanding the influence of wall excitation on the fluid dynamics within the microchannel. Fick's equation is integrated into the system above of equations to investigate the concentration distribution, enabling the extraction of the concentration distribution parameter. Equation (9) illustrates Fick's law, which describes the diffusion process and provides insights into how solute concentration varies within the flow field. This comprehensive approach facilitates a thorough analysis of the interaction between acoustic waves, fluid dynamics, and mass transport phenomena in microfluidic systems.

$$\frac{\partial c}{\partial t} + v_x \frac{\partial c}{\partial x} + v_y \frac{\partial c}{\partial y} + v_z \frac{\partial c}{\partial z} = D\left[\frac{\partial^2 c}{\partial x^2} + \frac{\partial^2 c}{\partial y^2} + \frac{\partial^2 c}{\partial z^2}\right] + R, \tag{9}$$

To analyze the concentration variations, boundary conditions of 1 $\mathrm{mol/m^3}$ and 0 $\mathrm{mol/m^3}$ were applied at the inlets of the micromixer. These conditions simulate the introduction of different fluid streams, enabling the investigation of how the mixing efficiency evolves within the microchannel. By establishing a concentration gradient, the study evaluates the effectiveness of the micromixing process, particularly under the influence of surface acoustic waves and flexible channel walls. The Lagrangian velocity magnitude ($\boldsymbol{v_{Lag}}$) resulting from solving the system of Eqs. (1) to (8) is applied to Fick's equation to extract the concentration distribution profile. The $\boldsymbol{v_{Lag}}$ is shown in the equation below.

$$\boldsymbol{v_{Lag}} = \boldsymbol{v_{Eul}} + < \frac{\boldsymbol{v}_1}{i\omega}.(\nabla \boldsymbol{v}_1) >, \tag{10}$$

Thus, Eqs. (1) to (9) result in the concentration distribution for two distinct types of acoustic-fluidic flow. The deformation of the Hyperelastic channel wall is analyzed using the two-parameter Mooney-Rivlin model, which characterizes the energy function of the solid body of the channel as follows. This approach allows for a detailed examination of how the channel wall's deformation affects the overall flow dynamics and concentration distribution, providing insights into the interaction between fluid mechanics and material properties in the micro-mixing process (Keerthiwansa 2020).

$$WS = C_{10}\left(\bar{I}_1 - 3\right) + C_{01}\left(\bar{I}_2 - 3\right), \tag{11}$$

where C_{10} and C_{01} are the model constants which are regarded as 0.25 and 0.05 *MPa* respectively, and $\bar{I}_1, \bar{I}_2$ are the first and second strain invariants, respectively. The effect of the Hyperelastic microchannel wall on mixing performance is investigated using the Arbitrary Lagrangian–Eulerian (ALE) theory (Berraies et al. 2404) to formulate the problem. A two-way fluid–structure interaction (FSI) (Xiao et al. 2024) coupling is implemented at the fluid–solid interface, allowing for a comprehensive analysis of the system's behavior. The selection of hyper-elastic materials for micromixing applications was guided by critical criteria to ensure optimal performance. These materials were required to exhibit significant elastic deformation under acoustic and fluid forces, enabling dynamic fluid–structure interactions (FSI) while maintaining mechanical integrity under repetitive loading cycles, such as surface acoustic waves (SAWs) and fluid-induced stresses. Additionally, compatibility with microfluidic fabrication techniques and chemical stability in biomedical and chemical environments were essential. The viscoelastic properties of these materials also played a role in dissipating unwanted resonances and ensuring effective wall deformations. Polydimethylsiloxane (PDMS) was chosen for its ability to meet these requirements and its proven application in microfluidics. The mechanical properties of hyper-elastic materials directly impact micromixing efficiency by facilitating deformation under acoustic pressure, which introduces dynamic changes in channel geometry, generates secondary flows, and enhances mixing. The elastic modulus of the material governs the extent of wall deformation, striking a balance between flexibility and structural integrity to promote efficient mixing. Furthermore, these materials effectively transfer acoustic energy into the fluid, creating vortices and secondary circulations, while their flexibility minimizes pressure drop by reducing resistance and accommodating fluid flow. Together, these properties significantly improve micromixing performance, enabling faster and more energy-efficient mixing within shorter channel lengths. The equations governing the problem are transferred to a numerical platform for solution. The efficiency of the mixing process is expressed using relation (12), which quantifies the effectiveness of the mixing under the influence of the Hyperelastic channel wall dynamics. This methodology provides valuable insights into the interactions between fluid mechanics and structural deformation, enhancing the understanding of mixing in microfluidic applications.

$$\eta = \left[1 - 2 * \sqrt{\frac{\int_A \left(\bar{c} - \bar{c}^*\right)^2 dA}{\int_A dA}}\right] \tag{12}$$

To examine the effects of the channel wall on the micromixing process inside the channel, the dimensionless number for the Hyperelastic thickness ($\lambda = \frac{W_H}{W}$) of the channel is considered. The dimensionless Peclet number is also used to analyze and understand the parametric mixing process in the fully coupled problem.

2.2 Material and parameters

The working fluid in the present study is water-based, and to examine viscosity variations, the Power-law model is adopted for shear-thinning, Newtonian, and shear-thickening fluid flows. To investigate the effect of thickness, the dimensionless parameter λ is considered. A parametric analysis is performed for the Power-law index (n), the Hyperelastic wall's dimensionless thickness, and the Peclet number. Table 1 shows the characteristics and parameters used in the present study. The values of the variables are presented in the table below with the notation [start, step, End].

2.3 Solution methodology

The current CFD investigation is carried out as a fully coupled fluid–structure interaction (FSI) analysis at the channel wall, specifically aimed at assessing the impact of the wall on the internal flow dynamics, employing the Arbitrary Lagrangian–Eulerian (ALE) framework. In this context, the acoustic-fluidic flow problem is systematically decomposed into three distinct perturbation levels: the zeroth-order background flow, which represents the primary fluid motion; the first-order acoustic response of the fluid, capturing the immediate effects of acoustic perturbations; and the second-order acoustic-fluidic interactions, which detail the nonlinear influences of the acoustic waves on the fluid behavior. Moreover, introducing a parametric power-law model transforms fluid behavior into a significantly nonlinear challenge, necessitating the solution of a complex system of nonlinear equations within the COMSOL numerical environment. After meticulously discretizing the geometry and validating the results for mesh independence, the findings are extracted and presented to emphasize their relevance to energy conversion mechanisms within microfluidic systems. This comprehensive approach enhances the understanding of how structural dynamics and fluid mechanics interplay, ultimately influencing energy transfer processes in engineered systems. The boundary conditions in this study were meticulously designed to realistically simulate real-world microfluidic applications. At the inlets, constant velocity conditions were applied to replicate steady fluid inflow, while zero-pressure conditions at the outlets ensured smooth egress, mirroring typical experimental setups. The lateral walls of the microchannel were subjected to acoustic excitation derived from surface acoustic wave (SAW) generator specifications, accurately representing fluid-acoustic interactions. Isothermal conditions were enforced on all channel walls to maintain uniform thermal effects, and continuity of stress and velocity was implemented at the fluid–solid interface to capture fluid–structure interactions (FSI) precisely. Numerical stability challenges, stemming from the strong coupling of fluid and solid domains in the Arbitrary Lagrangian–Eulerian (ALE) framework, were addressed using fine mesh refinement near the fluid–solid interface, validated through a grid independence study. Stabilization techniques, such as implicit solver coupling and relaxation parameters, mitigated convergence issues. Validation of boundary conditions and numerical methods through comparisons with analytical solutions and experimental data confirmed the model's ability to replicate the behavior of hyper-elastic materials and acoustic fields, ensuring its relevance and robustness for real-world applications.

2.4 Grid study

In the simulations conducted using non-Newtonian models and the effects of acoustic waves in microchannels, the analysis of mesh dependence is of critical importance. To ensure the independence of results, the mesh must be capable of accurately resolving the effects of thermal and viscous boundary layers. Specifically, the thickness of the viscous boundary layer δ_v is defined as follows:

$$\delta_v \sim \frac{\nu}{U}, \tag{13}$$

where ν is the kinematic viscosity and U is the mean flow velocity. In this study, considering the data which are given in Table 1 and under high-frequency excitation conditions ($f_0 = 1.94$MHz), the mesh should be configured to capture the wall displacement fluctuations accurately (d_0, see Table 1). These considerations highlight the necessity for an effective meshing strategy, including using layered meshes and determining the number of layers based on length and thermal scales to minimize mesh dependence and achieve optimal mixing and flow results in microchannels. Given that this parametric study focuses on the excitation of acoustic waves (d_0) and viscosity effects, the mesh resolution must also be selected parametrically to ensure accurate capturing of wall displacement in each numerical solution. For accurate simulations, the boundary layer thickness (δ_v) must be adequately resolved, as it varies based on changes in viscosity and flow conditions. Multiple grid configurations were tested to achieve mesh independence, and the results were compared to assess their impact on solution accuracy. The independence of the results from the mesh was confirmed by monitoring key flow variables, including the wall displacement and velocity profiles, with finer meshes converging to stable results. The results demonstrated that further mesh refinement did not significantly affect the calculated acoustic streaming fields or micromixing efficiency. The Womersley number, a key parameter for characterizing unsteady flow behavior in the presence of oscillating walls, was also monitored to ensure proper resolution within the boundary layer. The final mesh configuration was selected to balance computational cost and solution accuracy, ensuring the accurate

representation of acoustic and fluid dynamic phenomena. The mesh independence study thus confirmed the reliability of the numerical results, ensuring that the selected mesh could adequately capture the complex interactions between the flow field, acoustic waves, and species transport, particularly in regions near the wall where viscous effects dominate. Considering that the Lagrangian velocity field was used as the velocity input into the Fick equation to extract the concentration profile, and given that the mixing efficiency was measured based on this concentration profile, mixing efficiency can be considered an appropriate parameter for evaluating mesh independence. Examining how the mixing efficiency varies with different mesh resolutions makes it possible to assess whether the computational results are sufficiently independent of mesh size. If the mixing efficiency converges and shows negligible variation with finer meshes, the mesh is sufficiently refined and the numerical solution is reliable. Therefore, the mixing efficiency is a robust indicator for ensuring mesh independence in the present study.

Table 2 and Fig. 3 respectively illustrate the mesh type based on element count and the mesh independence study for mixing efficiency. The mixing efficiency parameter, obtained from the Multiphysics coupling in this study, reaches a stable state after Mesh Type 5, which has thus been selected as the optimal mesh for the numerical solution in this analysis.

2.5 Validation

To verify the accuracy of the present results, a comparative analysis was conducted with a prior study that numerically investigated non-Newtonian power-law fluid mixing in a rigid-walled channel (Faradonbeh et al. 2022) under similar acoustofluidic conditions (See Fig. 4). Notably, the referenced study itself demonstrated robust validation of its acoustofluidic methodology against the numerical work of Müller et al. (2012), ensuring the reliability of its findings. When the rigid channel assumption was implemented in the current framework, the results aligned closely with those reported in the aforementioned study, as illustrated in the figure below. This agreement underscores the validity of the present methodology and confirms its consistency with established numerical approaches (Fig. 4).

Table 2 Mesh types for independency study

Mesh type	Number of meshes	η
1	41,485	52.01
2	70,896	64.25
3	118,410	81.3
4	177,410	88.3
5	300,034	95.42
6	303,645	95.45

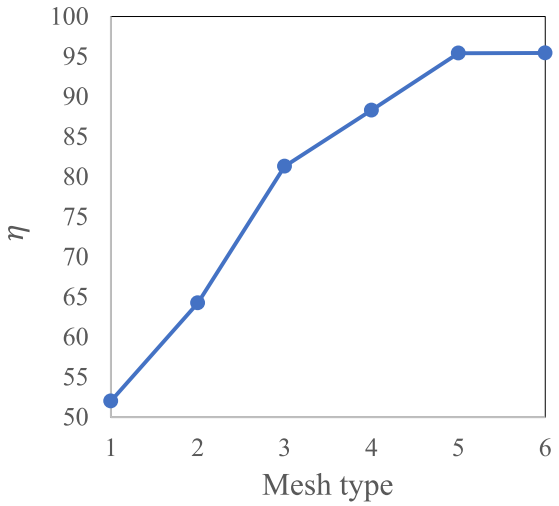

Fig. 3 Mesh independency study

3 Results

3.1 Concentration profile along the micromixer unit

Figures 5 and 6 showcase the concentration profiles of a micromixer unit with two different wall conditions: flexible ($\lambda = 1$) and rigid walls ($\lambda = 0$), at a Peclet number of 380 and a power-law index of 1.2. Using hyper-elastic materials for the channel walls, we significantly reduce the channel length needed to achieve optimal micromixing, enhancing the mixing efficiency from 0.8 to 0.99, as indicated in Eq. 12. Introducing surface acoustic waves (SAWs) disrupts the typical

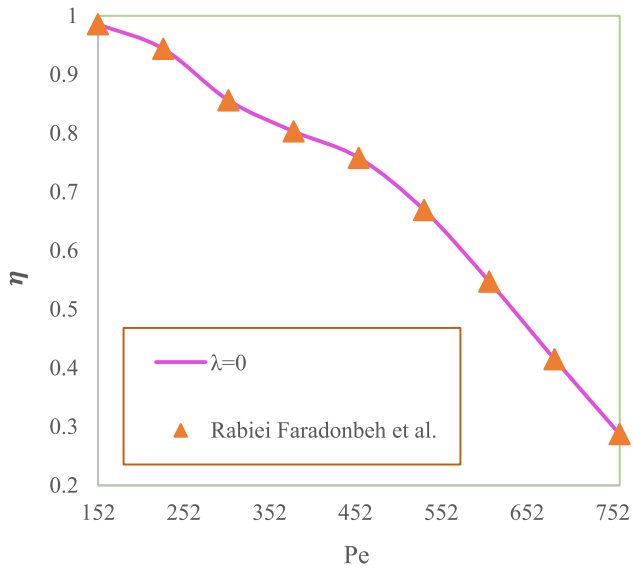

Fig. 4 Validation to Rabiei Faradonbeh et al. (2022)

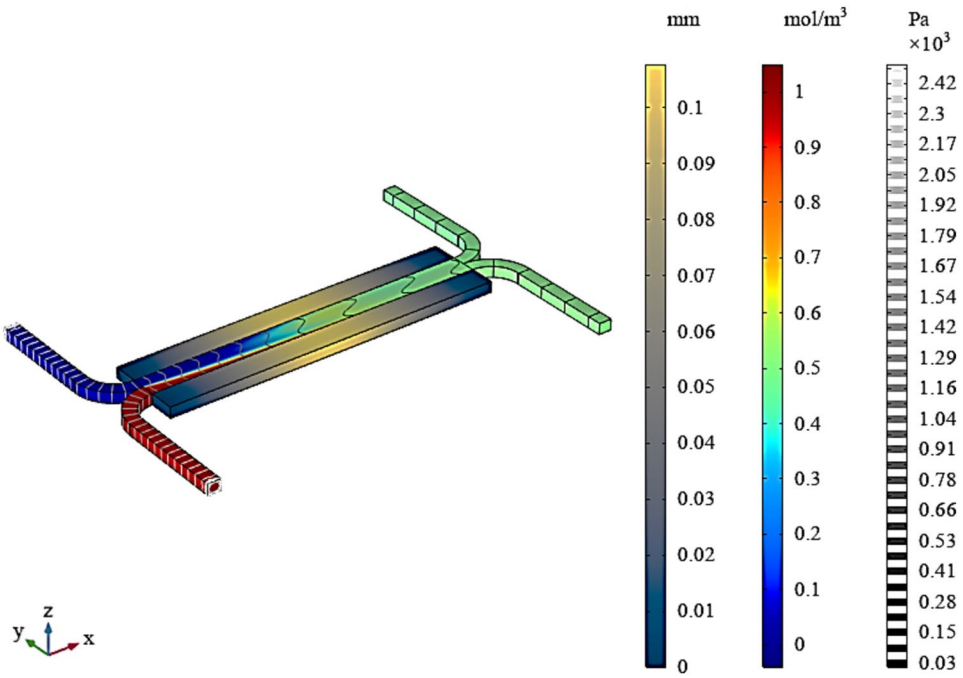

Fig. 5 Concentration profile of micromixer unit ($Pe = 380$, $n = 1.2$, $\lambda = 1$)

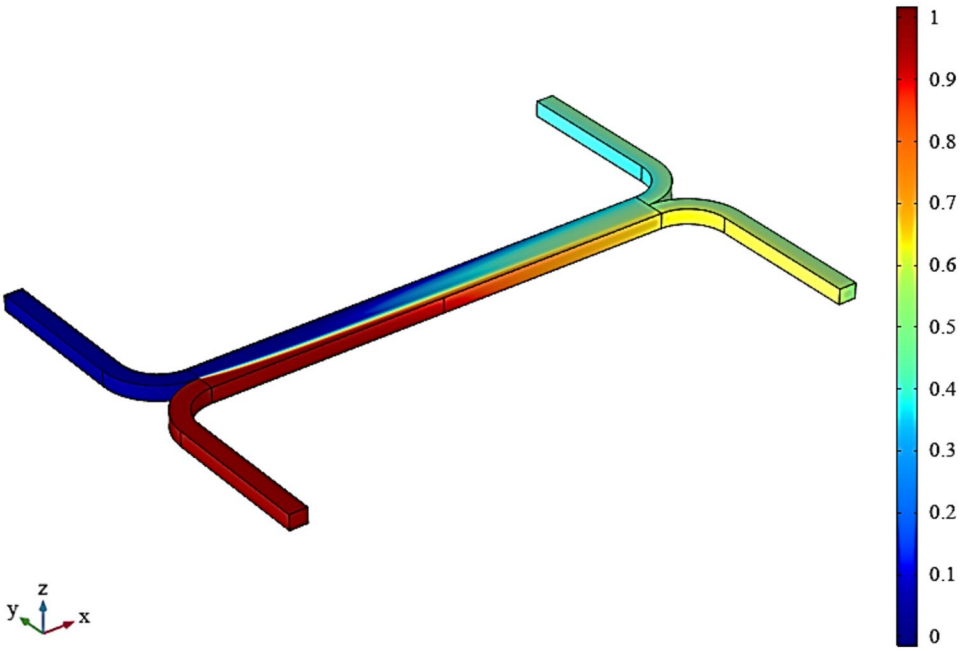

Fig. 6 Concentration profile of micromixer unit with rigid walls ($Pe = 380$, $n = 1.2$, $\lambda = 0$)

laminar flow, creating localized instabilities essential for improving mixing performance. Incorporating a Lagrangian velocity term in the modified governing equations enhances flow disruption, leading to more effective micromixing. Additionally, the combination of hyper-elastic channel walls and SAW-induced disturbances boost mixing efficiency over a shorter channel length, thus optimizing micromixer design. The hyper-elastic walls generate shear stresses at the fluid-wall interface, which are transferred as normal forces to the working fluid, further enhancing flow disturbances and mixing efficiency. This interaction between wall elasticity and SAW-induced disturbances is crucial for optimizing micromixer performance, allowing for shorter operational lengths while maintaining high efficiency. These findings highlight the importance of using hyper-elastic materials in micromixer designs, paving the way for future mechanical engineering and microfluidics innovations.

3.2 First-order acoustic fields

Figures 7 and 8 present the first-order fluid response fields to surface acoustic waves (SAWs). Specifically, Fig. 7 shows the first-order acoustic velocity field at the central cross-section of the channel, while Fig. 8 illustrates the velocity distribution along the channel's length. These results were derived from the thermo-viscous Eqs. (4–6) under boundary conditions. The velocity field increases from zero at the channel walls to a peak of 164 mm/s at the channel center. This symmetric distribution of the first-order velocity field is attributed to the application of two half-waves from the side walls of the channel. The figures also capture the response of a dilatant fluid, modeled as blood with a power-law index of $n = 1.2$, to the imposed acoustic waves. While blood is generally recognized as a shear-thinning fluid with viscoelastic properties under most physiological conditions, specific high-shear-rate scenarios, such as those encountered in acoustofluidic systems, can cause it to exhibit shear-thickening behavior. In these extreme conditions, the aggregation and disaggregation dynamics of red blood cells (RBCs), along with plasma protein interactions, lead to a temporary increase in apparent viscosity, aligning with the characteristics of a dilatant fluid. This study models blood using a power-law fluid with an index $n = 1.2$, representative of shear-thickening behavior, to capture the effects of these high-shear-rate conditions. This modeling approach provides valuable insights into micromixing performance under unique acoustofluidic scenarios and offers a comparative framework for evaluating performance differences between shear-thinning and shear-thickening fluids. By explicitly addressing this context, the study ensures that the rationale for this assumption is clear and grounded in relevant high-frequency microfluidic phenomena. As illustrated in Fig. 8, the fluid's response to the SAWs differs between the channel entrance and exit due to the interaction between the viscosity effect of fluid flow and acoustic waves, highlighting the localized variations in acoustic effects along the channel.

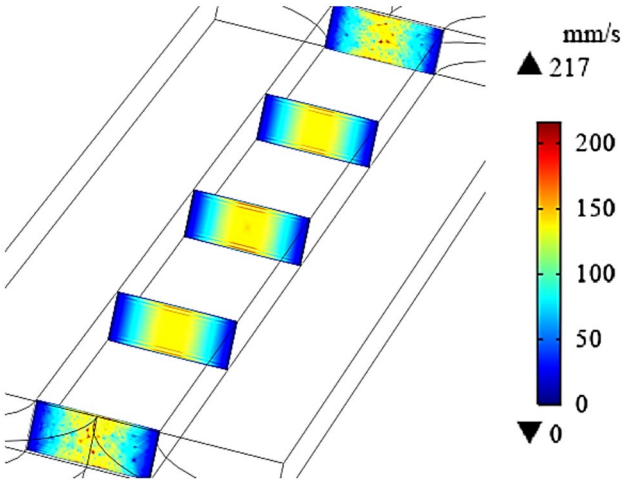

Fig. 8 Instantaneous local velocity ($Pe = 380$, $n = 1.2$, $\lambda = 1$)

Figures 9 and 10 illustrate the first-order acoustic pressure fields, with Fig. 9 showing the distribution at the mid-section of the channel and Fig. 10 depicts the variation along the channel's length. The symmetric pressure contours, derived from the governing Eqs. (4–6), result from applying half acoustic waves to each of the channel's side walls. This symmetric pressure profile along the micromixer unit plays a crucial role in practical applications, as it induces a centripetal force that drives viscous microfluidics toward the channel center. This mechanism significantly enhances the mixing efficiency by promoting a uniform distribution of fluid particles across the cross-section, optimizing micromixing performance.

Coupling the energy equation with the system of equations governing the fluid's frequency response to acoustic

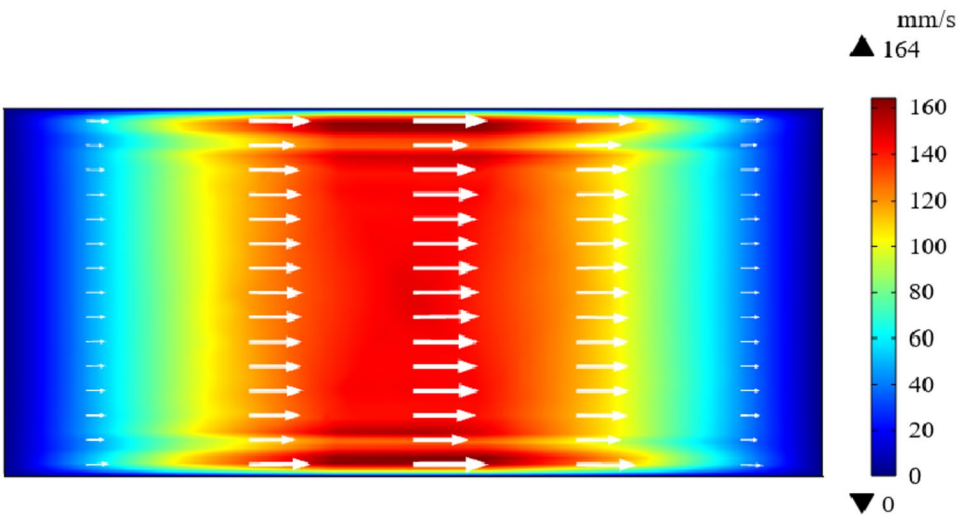

Fig. 7 First-order acoustic velocity at the center of channel cross section ($Pe = 380$, $n = 1.2$, $\lambda = 1$)

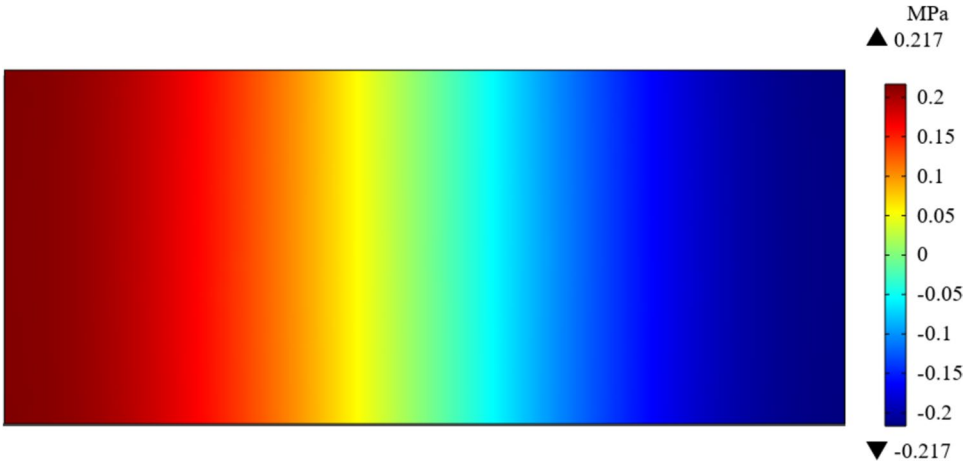

Fig. 9 First-order acoustic pressure at the center of the channel ($Pe = 380$, $n = 1.2$, $\lambda = 1$)

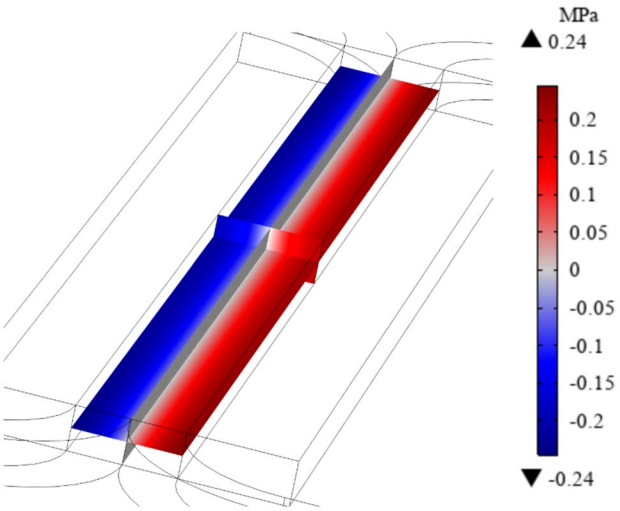

Fig. 10 Total acoustic pressure ($Pe = 380$, $n = 1.2$, $\lambda = 1$)

waves has produced the temperature profile presented in Fig. 11. Despite applying a constant temperature boundary condition, as defined in Eq. (4), to the channel walls, viscous interactions and the influence of acoustic waves have led to a localized temperature rise. Specifically, a slight temperature increase of approximately 5.3 mK is observed along the side walls where the fluid excitation boundary condition is applied. This thermal effect, though minimal, highlights the interaction between acoustic energy and viscous dissipation within the micromixer.

3.3 Second-order acoustic streaming

Figure 12 presents the second-order acoustic flow velocity, which integrates the continuity and Navier–Stokes equations under surface acoustic waves (SAWs) influence. In the main section of the microchannel where the SAWs are applied, a significant increase in flow velocity is observed, with the maximum second-order velocity reaching approximately 5.58 mm/s, as derived from the governing Eqs. (7) and (8) and the corresponding boundary conditions. Notably,

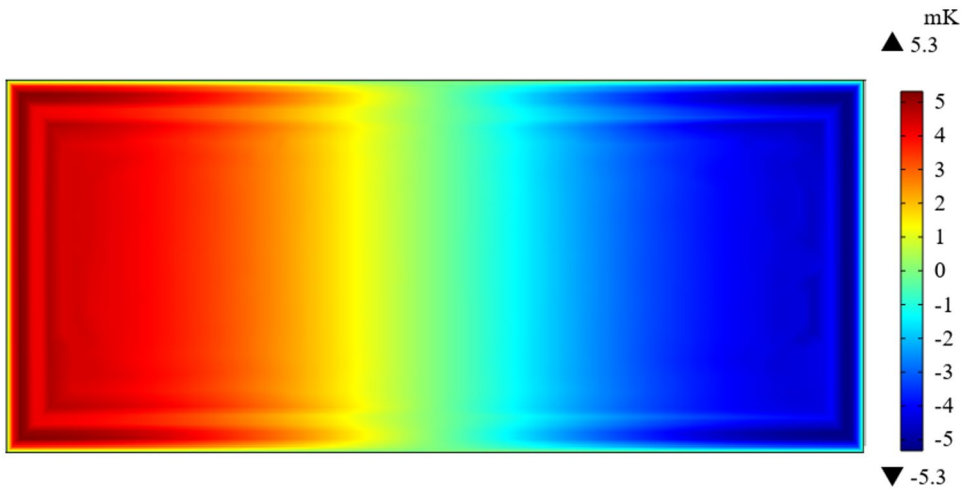

Fig. 11 Temperature gradient ($Pe = 380$, $n = 1.2$, $\lambda = 1$)

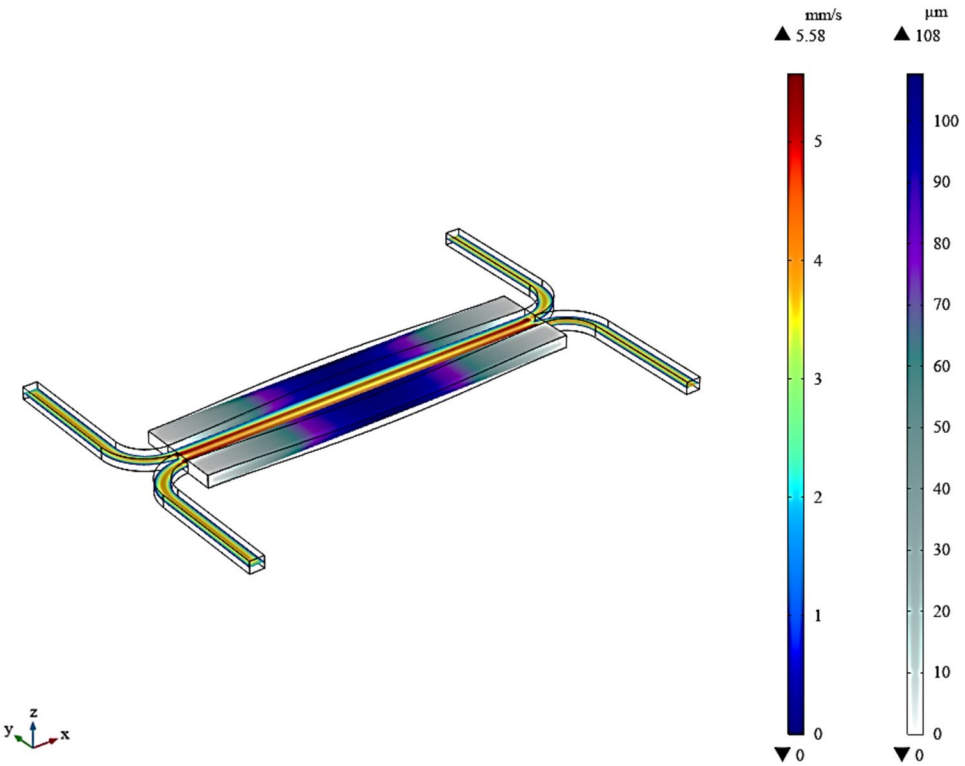

Fig. 12 Second-order acoustic streaming velocity in the Hyperelastic channel ($Pe = 380$, $n = 1.2$, $\lambda = 1$)

a reduction in flow velocity occurs at the channel center, attributed to forming a pressure node in this region. The flow dynamics around this pressure node exhibit a distinct roll-like pattern, illustrating the complex interaction between acoustic fields and fluid motion within the microchannel.

The application of SAWs, symmetrically applied as boundary conditions to the channel's side walls, induces the formation of a flow node at the channel center. Various flow species circulate in a rolling pattern around this pressure node, which enhances the mixing efficiency and overall performance of the micromixer unit. Figure 13 illustrates the flow roll and the mechanism by which this pattern increases mixing efficiency for a power-law index of 1.2, assuming fully viscous fluid behavior, alongside a Peclet number of 380 and a dimensionless thickness of 1. As Part A of the results section discussed, the hyper-elastic body generates normal forces on the fluid, improving mixing efficiency and mitigating the risk of fluid entrapment within the viscous boundary layer.

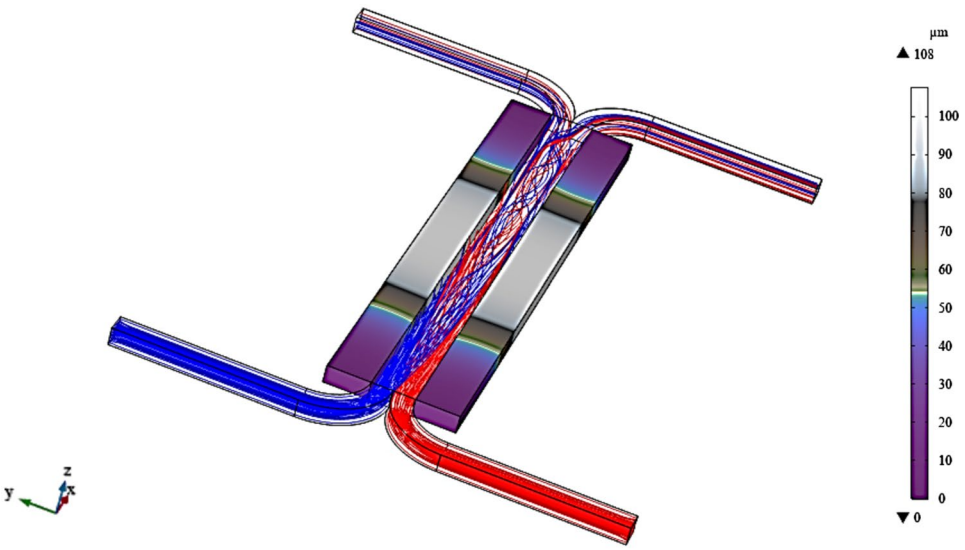

Fig. 13 Streamlines ($Pe = 380$, $n = 1.2$, $\lambda = 1$)

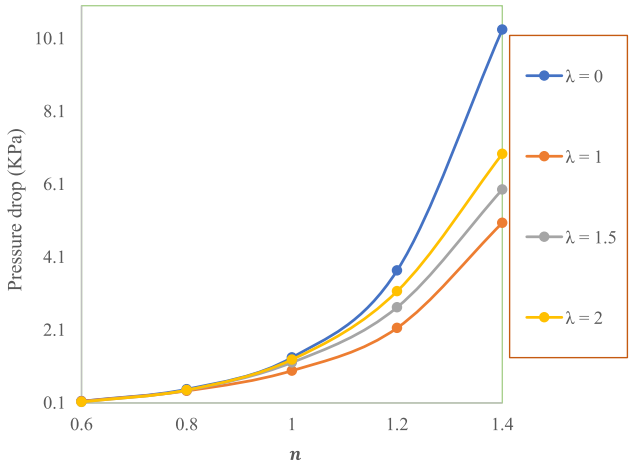

Fig. 14 Relation between pressure drop and n

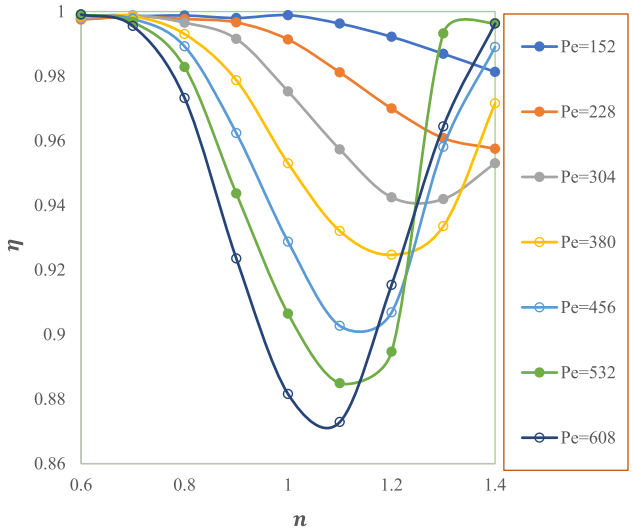

Fig. 15 $\eta - n$ plot for different Pe

3.4 Effect of wall flexibility on pressure drop

Figure 14 investigates the impact of viscosity on the pressure drop within the microchannel. The parameter $\lambda = 0$ signifies the rigid wall configuration. As illustrated, transitioning from a rigid channel wall to a hyper-elastic material results in a notable reduction in pressure drop along the micromixer channel. Generally, the data indicates that the pressure drop is more significant in channels with rigid walls than those with flexible walls. Conversely, introducing hyper-elastic wall material leads to an immediate decrease in pressure drop; however, increasing the dimensionless thickness of the channel subsequently increases pressure drop. It can be posited that the greater the fluid's capacity to exert shear stress on the channel walls—facilitated by high-viscosity fluids and channels of reduced thickness—the more pronounced the deformation of the wall. This deformation generates normal stresses transmitted back to the working fluid within the microchannel, enhancing mixing efficiency and minimizing the risk of fluid entrapment in the viscous boundary layer, thereby reducing pressure drop. Ultimately, incorporating fluid–structure interaction (FSI) phenomena in the micromixer channel design enables it to function similarly to a pump, propelling the fluid forward.

3.5 Relation between mixing efficiency and power law index

The concurrent application of fluid–structure interaction (FSI) and acoustofluidics has rendered the problem highly nonlinear. Figure 15 displays the $\eta - n$ diagram for the current investigation, illustrating the variations in mixing efficiency as a function of the viscosity parameter. The behavior of the graph stems from the complete coupling of multiple physical phenomena, transforming the problem into a fully coupled Multiphysics system. As depicted, an increase in the power-law index correlates with a reduction in mixing efficiency. This trend becomes more pronounced with an increase in the Peclet number due to the dominance of advective fluid motion over diffusive transport. Notably, the $\eta - n$ curve reveals a minimum value beyond which an upward trend is observed. This phenomenon can be attributed to the increased viscosity of the channel wall, which induces more significant shear stress and consequently enhances the return force exerted by the wall onto the fluid. This interaction disrupts the fluid motion more effectively, thereby improving mixing efficiency. Furthermore, the minimum point on the curve shifts to the right with a decrease in the Peclet number, indicating a coupling effect between FSI and the reduced decline in diffusive motion as the Peclet number decreases.

3.6 Vorticity magnitude relation with power-law index

Figure 16 illustrates the relationship between vorticity magnitude and the power-law index. As depicted, an increase in the power-law index corresponds to a decrease in the vorticity magnitude of the fluid. This trend arises because a higher power-law index increases fluid viscosity, which diminishes the ability of acoustic waves to generate flow rolls along the channel. A critical insight of this study is that, despite the formation of weaker flow rolls at elevated power-law indices, the everyday stresses transmitted back to the fluid effectively compensate for this reduction in mixing efficiency.

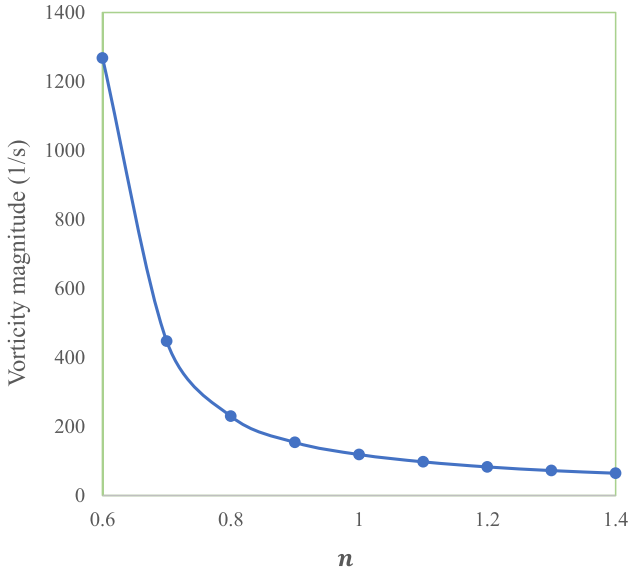

Fig. 16 Vorticity magnitude relation between n ($Pe = 380$, $\lambda = 1$)

3.7 $\eta - Pe$ for different lambda

Figure 17 examines the relationship between mixing efficiency and the Peclet number across different channel thicknesses. The overall declining trend observed in all curves is attributed to the increase in the Peclet number, which enhances the directed flow of the fluid relative to its diffusive motion. Curves corresponding to rigid walls and dimensionless thicknesses between 2.5 and 3.5 exhibits a pronounced reduction in disturbances caused by Acoustofluidic flow. In contrast, mixing efficiency initially reaches a minimum of 1.5 and 2 for wall thicknesses before demonstrating an upward trend as the Peclet number increases. This behavior is due to the increased flow velocity associated with higher Peclet numbers, which amplifies the fluid–structure interaction (FSI) mechanisms that enhance mixing efficiency. Specifically, for the 1.5 thickness, as shown in the figure, after reaching its minimum, the rise in flow velocity—previously perceived as detrimental to micromixing—is now effectively harnessed to achieve improved mixing outcomes, representing a significant finding of this study. Regarding the curve for the thicker walls, which displays a substantial upward shift in mixing efficiency, this phenomenon can be attributed to the full coupling between the fluid and the solid structures at the channel walls. In this scenario, the fluid cannot induce bulging in the walls, while the walls may bulge inward, effectively directing the fluid toward the channel center. However, this behavior falls outside the primary objectives of this research, and the potential for a significant pressure drop along the micromixer channel renders this outcome less desirable for the present study.

3.8 Concentration changes along the y-axis at the center of the channel

Figure 18 analyzes the concentration variations along the y-axis at the midsection of the channel for power-law indices spanning shear-thinning, Newtonian, and shear-thickening fluids. As the power-law index increases from 0.8 to 1.4, the rate of concentration variation also escalates. These disturbances in concentration profiles are primarily attributed to interactions with the acoustic waves. Notably, as the power-law index rises, both the peak height of the concentration curve and the graph's amplitude expand at the start and end points. This behavior results from the viscous fluid's

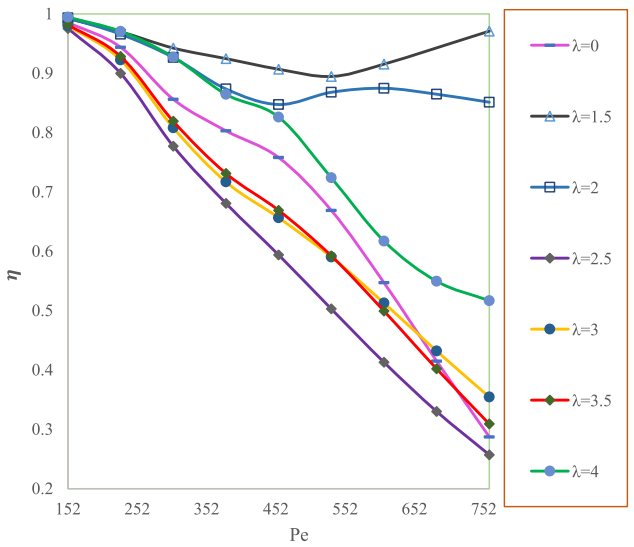

Fig. 17 $\eta - Pe$ plot for different λ

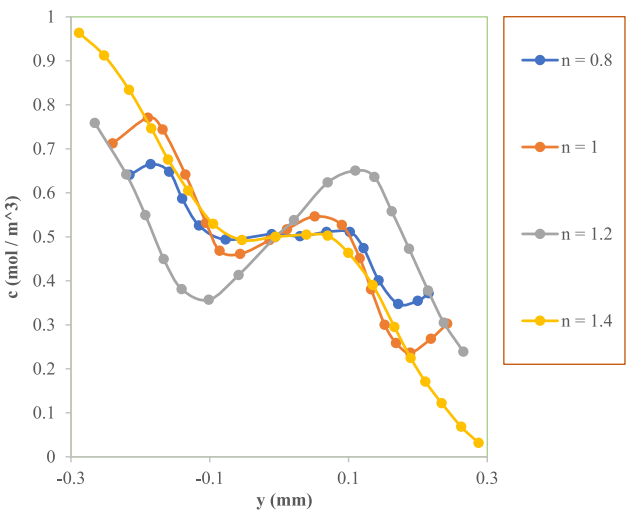

Fig. 18 Concentration difference at the center of the channel

capacity to induce deformation in the channel walls, further influencing the mixing dynamics within the system.

3.9 Von mises stress on microchannel body

The figure below illustrates the von Mises stress distribution applied to the channel wall. As indicated by the coupling of fluid–structure interaction (FSI) between the channel wall and the fluid flow results in stress being exerted on the channel wall. This stress peaks at 91.5 kN/m^2 at both the entrance and exit of the channel, coinciding with the fixed points of the wall. Accounting for these stress concentrations is essential in practical design considerations to ensure structural integrity and performance (See Fig. 19).

3.10 Total displacement for different Peclet numbers

Figure 20 illustrates the maximum displacement of the channel wall as the power-law index increases across various Peclet numbers. The figure demonstrates that an increase in the power-law index correlates with a more significant displacement of the channel wall. Additionally, an increase in the Peclet number further amplifies this displacement. As previously discussed, the higher Peclet number, which leads to increased directed flow velocity, results in more significant shear stress on the wall. This shear stress, in turn, is transmitted back to the fluid as normal stresses. Interestingly, while a rise in the Peclet number was initially viewed as a challenge to enhancing mixing efficiency, it has emerged as a beneficial factor in this context.

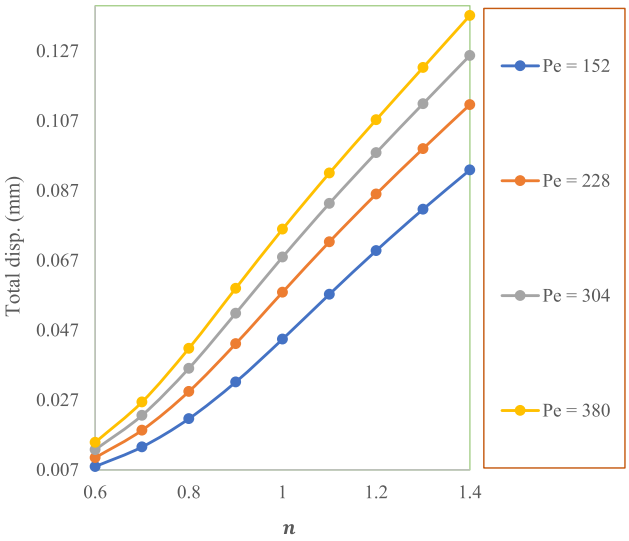

Fig. 20 Relation between wall displacement and power-law index

4 Conclusion

This study presents a comprehensive investigation into the performance of a micromixer utilizing hyper-elastic materials and surface acoustic waves (SAWs) for enhanced micromixing efficiency. The results demonstrate a remarkable

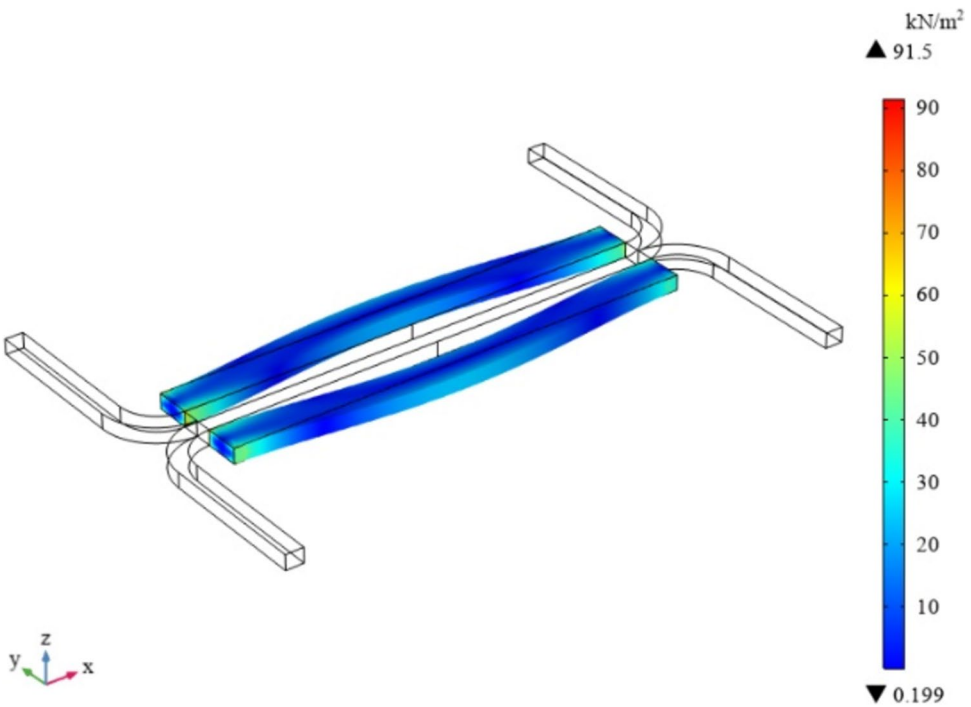

Fig. 19 Von Mises stress on channel walls ($vel = 0.005$m/s and $n = 1.2$)

improvement in mixing efficiency from 0 to 0.99, achieved through the innovative combination of flexible channel walls and SAW-induced disturbances. This advancement allows for a significant reduction in the channel length required for optimal mixing, thereby enhancing micromixer design and functionality. The analysis of concentration profiles revealed that introducing SAWs disrupts the conventional laminar flow, creating localized instabilities that are critical for improving mixing performance. The symmetric distribution of the first-order acoustic velocity field, characterized by peak velocities of 164 mm/s at the channel center, illustrates the effective response of a dilatant fluid, modeled as blood with a power-law index of $n = 1.2$, to the applied acoustic waves. The findings highlight the complex interplay between fluid viscosity, acoustic pressure fields, and the resulting flow dynamics, particularly the formation of pressure nodes that facilitate enhanced mixing. The study extensively highlights the role of fluid–structure interaction (FSI) in significantly improving micromixing efficiency within microchannels. The interaction between the hyper-elastic channel walls and the fluid generates dynamic wall deformations, which in turn induce secondary flows and localized disturbances in the primary flow. These effects are especially pronounced at low Reynolds numbers, where achieving efficient mixing through conventional methods is challenging. The deformable channel walls increase the surface area available for fluid interaction, promoting enhanced diffusion and faster homogenization of fluid layers, particularly for non-Newtonian fluids. Additionally, FSI facilitates nonlinear flow behavior, including the stretching and folding of fluid elements, which further augments mixing efficiency. This study demonstrates that the use of hyper-elastic walls not only reduces pressure drop but also optimizes fluid motion, providing a pathway for designing advanced micromixers with tailored wall properties to achieve superior mixing performance in shorter operational lengths. This reduction is attributed to the channel's ability to adaptively respond to fluid stresses, thereby mitigating the risk of fluid entrapment within viscous boundary layers. The $\eta - n$ diagram elucidated a nonlinear relationship between mixing efficiency and the power-law index, revealing that while higher viscosity initially reduces mixing efficiency, the compensatory mechanisms of shear stress transmission effectively enhance overall performance. Additionally, the study found that the interaction between SAWs and fluid viscosity critically influences the acoustic flow rolls, further highlighting the importance of tuning these parameters for optimized micromixing.

The scalability of the proposed micromixer design for industrial applications lies in its modular nature and reliance on surface acoustic wave (SAW) technology. To transition from laboratory-scale to large-scale use, several factors must be addressed, including optimizing SAW generator designs to maintain energy efficiency, enhancing material durability for aggressive industrial environments, and adapting channel dimensions to accommodate higher throughput while preserving mixing efficiency. Modifications such as employing advanced piezoelectric materials for stronger and uniform acoustic wave generation, reinforcing hyper-elastic channel walls to withstand higher flow rates, and implementing parallel channel configurations for increased fluid volumes would be necessary. Additionally, integrating real-time monitoring and control systems could dynamically adjust mixing parameters to optimize performance under varying conditions. While this study focuses on numerical simulations, plans for experimental validation include testing the micromixer with biological fluids in biomedical applications, such as diagnostic assays or drug delivery systems, and evaluating metrics like mixing efficiency and cell viability to ensure compliance with stringent requirements. Prototyping and fabrication using microfabrication techniques will bridge the gap between simulation and practical implementation. The compact and energy-efficient design, coupled with the adaptability of hyper-elastic materials, makes this micromixer particularly suited for biomedical and industrial applications, paving the way for its widespread adoption with further validation and targeted modifications.

In summary, the integration of hyper-elastic materials and acoustofluidics within micromixer designs represents a significant advancement in the field of microfluidics and mechanical engineering. Future research should focus on exploring the long-term stability and performance of hyper-elastic materials under varying operational conditions, as well as the scalability of this technology for industrial applications. Moreover, investigating the effects of different fluid properties and geometrical configurations will be essential in further refining micromixing strategies, thereby paving the way for innovative applications in biomedical engineering, chemical processing, and beyond.

Author contributions All authors reviewed the manuscript.

Data availability No datasets were generated or analysed during the current study.

Declarations

Conflict of interest The authors declare no competing interests.

References

Ababneh J et al (2023) Evaluating the mixing performance in a planar passive micromixer with T-shape and SAR mixing chambers: comparative study. In: 2023 2nd International Engineering Conference on Electrical, Energy, and Artificial Intelligence (EICEEAI). IEEE

Afzal A et al (2021) Active and passive micromixers. Analysis and Design Optimization of Micromixers, pp 11–34
Ang B et al (2023) Glass-embedded PDMS microfluidic device for enhanced concentration of nanoparticles using an ultrasonic nanosieve. Lab Chip 23(3):525–533
Babaie Z, Bahrami D, Bayareh M (2022) Investigation of a novel serpentine micromixer based on Dean flow and separation vortices. Meccanica 57(1):73–86
Bahrami D, Bayareh M (2022) Impacts of channel wall twisting on the mixing enhancement of a novel spiral micromixer. Chem Papers. https://doi.org/10.1007/s11696-021-01876-5
Bai C et al (2022) A surface acoustic wave-assisted micromixer with active temperature control. Sens Actuators, A 346:113833
Bai C et al (2024) Acoustohydrodynamic micromixers: basic mixing principles, programmable mixing prospectives, and biomedical applications. Biomicrofluidics. https://doi.org/10.1063/5.0179750
Bansal AK et al (2023) Micromixing optimization of non-newtonian fluids with heterogeneous zeta potential. Eng Res Express 5(3):035031
Bayareh M, Ashani MN, Usefian A (2020) Active and passive micromixers: a comprehensive review. Chem Eng Process-Process Intensific 147:107771
Bazaz SR et al (2024) Micromixer research trend of active and passive designs. Chem Eng Sci 293:120028
Berraies AA, van Brummelen EH and Auricchio F (2024) Numerical investigation of fluid-structure interaction in a pilot-operated microfluidic valve. arXiv preprint arXiv:2404.18335
Cha B et al (2023) Rapid acoustofluidic mixing by ultrasonic surface acoustic wave-induced acoustic streaming flow. Ultrasonic Sonochem 99:106575
Chen C et al (2018) Passive mixing inside microdroplets. Micromachines 9(4):160
D'Avino G, Maffettone PL (2022) Effect of wall slip on the viscoelastic particle ordering in a microfluidic channel. Electrophoresis 43(21–22):2206–2216
Dhulipala SL et al (2022) Development, verification, and validation of comprehensive acoustic fluid-structure interaction capabilities in an open-source computational platform. Earthq Eng Struct Dyn 51(10):2188–2219
Faradonbeh VR et al (2022) Power-law fluid micromixing enhancement using surface acoustic waves. J Mol Liq 347:117978
Farahinia A et al (2021) Numerical analysis of the heterogeneity effect on electroosmotic micromixers based on the standard deviation of concentration and mixing entropy index. Micromachines 12(9):1055
Ferreira M et al (2024) Advances in microfluidic systems and numerical modeling in biomedical applications: a review. Micromachines 15(7):873
Ghorbani Kharaji Z, Bayareh M, Kalantar V (2021) A review on acoustic field-driven micromixers. Int J Chem React Eng 19(6):553–569
Ghorbani Kharaji Z, Kalantar V, Bayareh M (2022) Acoustic sharp-edge-based micromixer: a numerical study. Chem Pap 76(3):1721–1738
Hussain A et al (2023) Hyper-elastic behavior of soft-tissue like microgels in two-phase converging microchannel flow. Phys Fluids. https://doi.org/10.1063/5.0174625
John T et al (2024) Viscoelastic flow asymmetries in a helical static mixer and their impact on mixing performance. J Nonnewton Fluid Mech 323:105156
Keerthiwansa R et al (2020) Hyperelastic material characterization: how the change in mooney-rivlin parameter values effect the model curve. Mater Sci Forum Trans Tech Publ. https://doi.org/10.4028/www.scientific.net/MSF.994.265
Kharaji ZG, Bayareh M (2024) Non-Newtonian fluid mixing in spiral micromixers: an extensive numerical analysis. Int Commun Heat Mass Transfer 158:107850
Kouadri A et al (2024) Assessment of mixing behaviors of non-Newtonian pseudoplastic fluids in short microdevices. Int Commun Heat Mass Transfer 155:107500
Kumar L and Pandey SK (2022) Design and optimisation of hyperelastic multi-axial strain and contact pressure sensor. In: 2022 IEEE 19th India Council International Conference (INDICON). IEEE
Lei J et al (2020) Numerical simulation of continuous separation of microparticles in two-stage acousto-microfluidic systems. Appl Math Model 83:342–356
Li T et al (2024) Fabrication of patterned magnetic particles in microchannels and their application in micromixers. Biosensors 14(9):408
Mahapatra B, Bandopadhyay A (2022) Efficacy of microconfined fluid mixing in a combined electroosmotic and pressure driven transport of complex fluid over discrete electrodes. Phys Fluids. https://doi.org/10.1063/5.0086541
Mahapatra B, Bandopadhyay A (2023) Experimental investigations on geometry modulated solute mixing in viscoelastic media. Ind Eng Chem Res 62(9):4095–4108
Meng Y, Wu Y (2023) Numerical characterization and optimization of the acoustic device for heterogeneous immunoassays. Microfluid Nanofluid 27(11):71
Mezzanzanica G et al (2022) A microfluidic device based on standing surface acoustic waves for sorting and trapping microparticles. Eng Proc 27(1):28
Muller PB (2012) Acoustofluidics in microsystems: investigation of acoustic streaming. Master's thesis, DTU Nanotech, Department of Micro-and Nanotechnology
Nalimela P et al (2025) Steady flow of thermo-viscous fluid between infinitely stretched porous parallel plates—a perturbation technique. CFD Lett 17(1):78–89
Oh S, Lee C-S (2024) Comparison and analysis of mixing efficiency in various micromixer designs. Korean J Chem Eng 46:5345
Peng L et al (2024) Electro-osmotic flow instability of viscoelastic fluids in a nanochannel. Phys Fluids. https://doi.org/10.1063/5.0233974
Qi X et al (2024) Optimal design of micromixer for preparation of nanoliposomes. Chem Eng Process-Process Intensific 196:109677
Quintard C et al (2022) Microfluidic device integrating a network of hyper-elastic valves for automated glucose stimulation and insulin secretion collection from a single pancreatic islet. Biosens Bioelectron 202:113967
Ramesh K, Mebarek-Oudina F, Souayeh B (2024) Mathematical modelling of fluid dynamics and nanofluids. CRC Press, Taylor & Francis Group, Boca Raton
Reichel F et al (2024) High-throughput viscoelastic characterization of cells in hyperbolic microchannels. Lab Chip 24(9):2440–2453
Rubio Martínez A et al (2024) Flow modeling of a non-newtonian viscous fluid in elastic-wall microchannels. Fluids 9(3):77
Saravanakumar SM, Cicek P-V (2023) Microfluidic mixing: a physics-oriented review. Micromachines 14(10):1827
Sasmal C (2022) A simple yet efficient approach for electrokinetic mixing of viscoelastic fluids in a straight microchannel. Sci Rep 12(1):2395
Solano-Arana S et al (2018) A novel application of dielectric stack actuators: a pumping micromixer. Smart Mater Struct 27(7):074008
Stevenson P (2024) QCD Perturbation Theory: It's not what you were taught. arXiv preprint arXiv:2409.01228
Takayama T, Kaneko M, Tsai C-HD (2021) On-chip micro mixer driven by elastic wall with virtual actuator. Micromachines 12(2):217
Usefian A, Bayareh M (2020) Numerical and experimental investigation of an efficient convergent–divergent micromixer. Meccanica 55(5):1025–1035

Usefian A et al (2019) Numerical study of electro-osmotic micro-mixing of Newtonian and non-Newtonian fluids. J Braz Soc Mech Sci Eng 41:1–10

Wang W, Zhang J and Xu C (2024) Oscillating feedback micromixer: a short review. Chem Eng Process -Process Intensific 201:109812

Xiao J et al (2024) A two-way coupled fluid–structure interaction method for predicting the slamming loads and structural responses on a stiffened wedge. Phys Fluids. https://doi.org/10.1063/5.0212806

Yin S (2023) Recent advances of the development and optimization design of passive microfluidic mixers. Highlight Sci Eng Technol 37:208–217

Zheng L et al (2024) Design, implementation, and optimization of a novel chaotic micromixer. Ind Eng Chem Res 63(32):14444–14457